TOXICOLOGICAL SCIENCES **126(2)**, 436–445 (2012)
doi:10.1093/toxsci/kfs007
Advance Access publication January 12, 2012

Intracellular Pb^{2+} Content Monitoring Using a Protein-Based Pb^{2+} Indicator

Tai-Yu Chiu*,† and De-Ming Yang*,†,[1]

*Institute of Biophotonics, School of Medical Technology and Engineering, National Yang-Ming University, Taipei 11217, Taiwan, Republic of China; †Department of Medical Research and Education, Taipei Veterans General Hospital, Taipei 11217, Taiwan, Republic of China

[1]To whom correspondence should be addressed. Fax: 886-2-2875-7435. E-mail: yang.deming@gmail.com.

Received September 22, 2011; accepted December 29, 2011

Lead ion (Pb^{2+}) is one of the most hazardous heavy metals to almost all life forms. The components of store-operated Ca^{2+} entry as a molecular gateway have been previously found to participate in the cytotoxic entry of Pb^{2+}. However, the safe levels of intracellular Pb^{2+} hiding in blood Pb^{2+} levels are still not determined with full certainty. The present study aimed to construct protein-based Pb^{2+} indicators to help establish a reliable setting for the content monitoring of intracellular Pb^{2+}. A series of Pb^{2+} indicators based on fluorescence resonance energy transfer, Met-leads, were developed. The Pb^{2+}-binding protein PbrR (from *Cupriavidus metallidurans* CH34) was applied between the fluorescent protein pair ECFP(ΔC11) and cp173Venus. The spectral patterns and sensing ranges of all Met-leads were characterized *in vitro*. Among these constructs, Met-lead 1.59 had relatively high ion selectivity and broad dynamic range (3.3–5.7). Consequently, this Met-lead was adopted in the cellular Pb^{2+} biosensing. The intracellular Pb^{2+} content in human embryonic kidney cells was successfully monitored using Met-lead 1.59 under both short- and long-term treatments. The existence of intracellular Pb^{2+} can be significantly sensed using Met-lead 1.59 after 3 h 0.5μM (10 μg/dl) exposure, which is 200 times more improved than previous live-cell indicators. In summary, a new Pb^{2+} indicator, Met-lead 1.59, was successfully developed for advanced research on Pb^{2+} toxicology.

Key Words: **FRET-based fluorescent Pb^{2+} indicator; intracellular Pb^{2+} monitoring; heavy metal ion biosensing; live-cell imaging; MerR.**

The heavy metal Pb^{2+} causes severe damage to almost all life forms and is therefore considered a notorious toxicant. Previous research has revealed that store-operated Ca^{2+} entry (SOCE) plays a dominant role in the cytosolic entry of Pb^{2+} (Chang *et al.*, 2008; Kerper and Hinkle, 1997), which is an important step in initiating Pb^{2+} toxicity. Recently, our group has found that the 106 position of Orai1/calcium release–activated Ca^{2+} channel protein 1 (CRACM1), together with stromal interaction molecule 1 (STIM1), is critical in selective ion gating during the cytotoxic entry of Pb^{2+} (Chiu *et al.*, 2009). However, whether Orai1/CRACM1–STIM1 is the only molecular gateway of extracellular Pb^{2+} entry is still presently inconclusive. On the clinical side, the blood Pb^{2+} level (BLL) of 10 μg/dl (Centers for Disease Control and Prevention [CDC], 1991) or approximately 0.5μM, has previously been thought as a cause for concern. However, this BLL has recently been noticed as underestimated and is suggested to be downward revised particularly for children (CDC Advisory Committee on Childhood Lead Poisoning Prevention, 2007). This situation implies that the acceptable Pb^{2+} concentration in a living environment, whether from an unexpected lead-containing diet or continuous occupational exposure, should be more carefully reconsidered. The safe levels of intracellular Pb^{2+} that actually provide more serious toxic information than BLL still remain uncertain.

To deal with the issues of Pb^{2+} entry (i.e., intracellular Pb^{2+} monitoring) and toxicity under unknown intracellular levels, some Pb^{2+} indicators have been produced chemically (e.g., indo-1 under specific emission wavelength) (Chen *et al.*, 2005; He *et al.*, 2006; Kerper and Hinkle, 1997; Marbella *et al.*, 2009) or genetically (Mizuno *et al.*, 2007; Richmond *et al.*, 2000). These indicators are capable of noninvasively sensing intracellular Pb^{2+}. However, they are limited in different ways, such as in terms of ion selectivity and signal sensitivity. Hence, their toxicological applications are limited. Taking indo-1 as a practical example, the photoinstability of indo-1 may cause a signal-judging problem in a Pb^{2+}-induced quenching out of photobleach. Indispensable Pb^{2+} indicators that can both monitor the Pb^{2+} content after long-term exposure and trace intracellular Pb^{2+} after cytotoxic entry need to be established. The first protein-based indicator, "cameleon," is built based on the detection of intramolecular fluorescence resonance energy transfer (FRET) between two green fluorescent protein (GFP) mutants, cyan fluorescent protein (CFP) and yellow fluorescent protein (YFP), to sense intracellular Ca^{2+} (Miyawaki *et al.*, 1997). Unfortunately, despite the fact that many important biomolecular indicators are created with inspiration from cameleon, quite few FRET sensors for detecting specific ions have been successfully

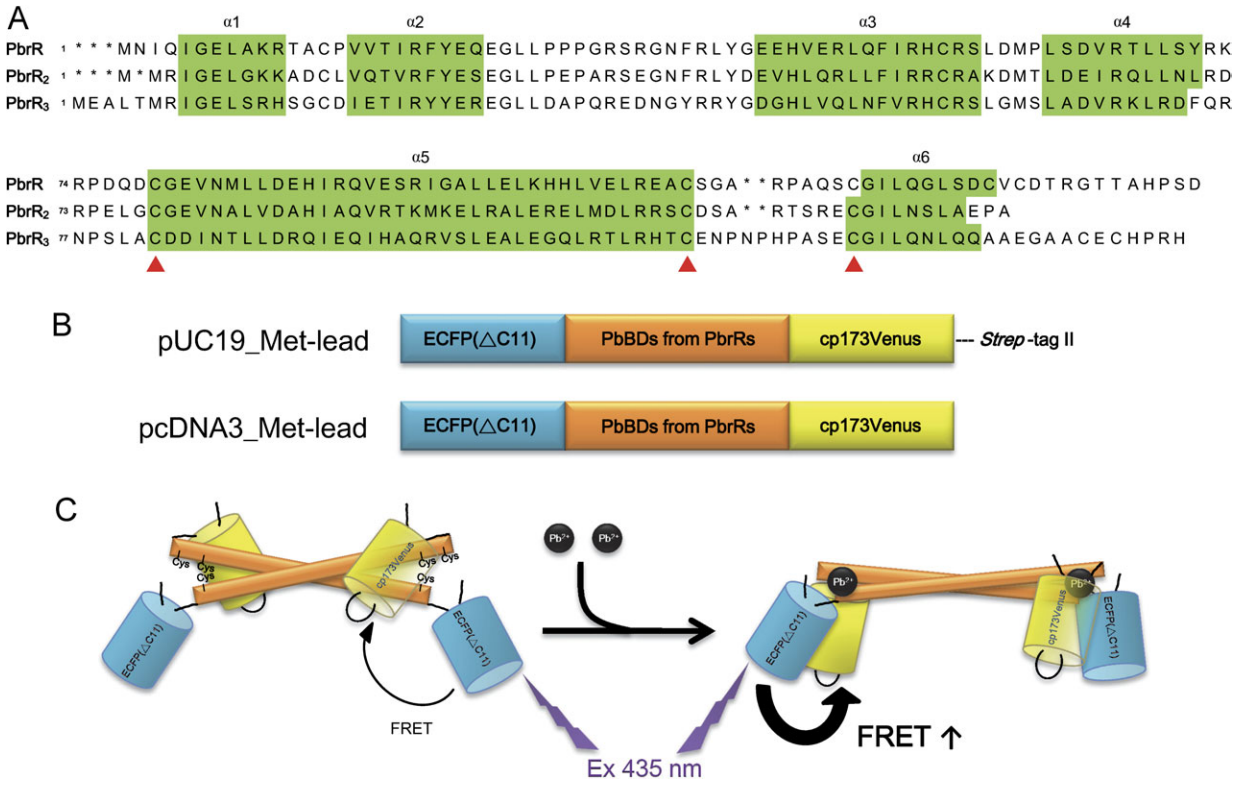

FIG. 1. Sequences of PbrRs and schematic design for constructing new lead indicators, Met-leads, through proposed functional structure changes between FRET pairs with the existence of Pb^{2+}. (A) Sequence alignments of three PbrR isoforms, including PbrR, $PbrR_2$, and $PbrR_3$, using the Kalign alignment tool (see Materials and Methods section). The shaded regions are the proposed secondary α-helix structures predicted by the PredictProtein program. The three cysteine residues marked with triangles are the sites hypothesized to bind the heavy metal Pb^{2+} coordinately. (B) The schematic design of the Pb^{2+}biosensor, Met-leads. PbBDs (center box; residues 59–131 from PbrR, residues 58–130 from $PbrR_2$, and residues 62–136 from $PbrR_3$), as sensing keys, contain the fourth (α4) to sixth (α6) α-helices of the PbrRs ligated between ECFP(ΔC11) (left box) and cp173Venus (right box). The expression vectors pUC19 and pcDNA3 were used in bacterial and mammalian cells. *Strep*-tag II was used for protein purification. (C) The proposed functional structure of Met-leads for Pb^{2+} sensing. The binding of Pb^{2+} to the three cysteine residues inside the PbBDs of the Met-leads and the shortened distance between ECFP(ΔC11) and cp173Venus increased the FRET signal.

developed (Li *et al.*, 2006). Most of these ion indicators are for Ca^{2+} (Miyawaki *et al.*, 1997; Nagai *et al.*, 2004), some are for Zn^{2+} (Vinkenborg *et al.*, 2010), and a very recent one is for Cu^{+} (Wegner *et al.*, 2010). The difficulty in fabricating such metal ion indicators is probably due to the lack of suitable sensing keys, i.e., the metal ion–binding proteins (MDPs). These MDPs can both precisely bind specific ions and dramatically perform conformational changes.

The present study aimed to build applicable protein-based Pb^{2+} indicators for cellular Pb^{2+} biosensing. Metalloregulatory proteins (PbrRs) originating from *Cupriavidus metallidurans* (previously named *Ralstonia metallidurans*) CH34 (Taghavi *et al.*, 2009) can specifically bind lead ions. Hence, PbrRs may be a suitable MDP for producing GFP-based Pb^{2+} indicators. Part of the PbrRs was incorporated into the FRET-GFP sensor backbone (Nagai *et al.*, 2004). A new series of Pb^{2+} indicators was successfully developed and named Met-leads. Using this unique sensing tool, the dynamic detection of cytotoxic Pb^{2+} entry and the content monitoring of Pb^{2+} in living cells during long-term exposure were investigated.

MATERIALS AND METHODS

Chemicals. All reagents were purchased from the Sigma Chemical Company (St Louis, MO) unless indicated otherwise. Most of the reagents for molecular cloning, e.g., restriction enzymes, ligases, etc., were from New England BioLabs. The polymerase chain reaction kit and primers were from Finnzymes (OY, Finland) and Mission Biotech (Taiwan), respectively. The DNA extraction kit was from Viogene.

Sequence alignment and gene construction. The gene alignment of the PbrR proteins shown in Figure 1A was performed using the multiple-sequence alignment algorithm of the Kalign program (European Molecular Biology Laboratory-European Bioinformatics Institute). The domain structures within the PbrRs were predicted as α-helices using the PredictProtein (Rost *et al.*, 2004). The Pb^{2+}-binding domain (PbBD) was proposed to contain the last three α-helix structures according to a previous study on the similar metal-binding domain of MerR (Zeng *et al.*, 1998). The PbBD gene fragments used in the present study as the Pb^{2+} sensing part were cloned from *C. metallidurans* CH34 (Changela *et al.*, 2003). The PbBDs, ECFP(ΔC11), and cp173Venus (Nagai *et al.*, 2004) were ligated together as the Met-leads. They were further cloned into different expression vectors (Fig. 1B). For protein purification and *in vitro* characterizations, Met-leads fused with *Strep*-tag II were cloned into pUC19 (Yeastern Biotech, Taiwan), forming pUC19_Met-leads. For cellular sensing applications, the constructs within the pcDNA3 vector (Invitrogen) were applied to form pcDNA3_Met-leads.

Expression and purification of Met-leads. The bacterial strain *Escherichia coli* BL21 (Yeastern Biotech) was cultured and transformed with the pUC19_Met-leads under isopropyl β-D-1-thiogalactoside induction.

The proteins of the Met-lead constructs with *Strep*-tag II were purified according to the protocol in the production manual with some modifications. Generally, the transformed bacteria were collected, resuspended under a 3-morpholinopropane-1-sulfonic acid (MOPS)-EDTA buffer (100mM MOPS, 150mM NaCl, 1% protein inhibitor, and 2mM EDTA; pH 8.0), and sonicated. The supernatant with the proteins were centrifuged and allowed to flow through a *Strep*-Tactin Spin Column (IBA GmbH, Gottingen, Germany). Elution by a MOPS eluting buffer (100mM MOPS, 150mM NaCl, and 4mM biotin; pH 7.2) followed. The protein concentration of the Met-leads was quantified by the Bio-Rad Protein Assay and the bovine serum albumin standard curve. The Met-leads were diluted by a MOPS buffer (100mM MOPS and 150mM NaCl; pH 7.2). A certain concentration of the Met-leads (1μM) was used for the fluorescent spectrum, ion selectivity, and ion competition analyses (within the same MOPS buffer).

In vitro *characterizations.* The diluted Met-lead proteins were placed on a 96 flat-bottom black polystyrol dish (Greiner). Generally, the total measuring procedure (including preparing 36–48 samples within a 96-well dish) consumes 30 min–1 h. The emission spectra (450–600 nm) of the Met-lead proteins were scanned at an excitation wavelength of 435 nm (with a 5 nm bandwidth) using a fluorescence spectrometer (Infinite M1000; TECAN, Switzerland). The step size was 1 nm, and the gain value was 140. The emission intensities at the 521–550 and 461–490 nm regions were used for the fluorescence intensity (FI) analyses of YFP and CFP, respectively, to calculate the FRET emission ratio (YFP/CFP).

Various Pb^{2+} concentrations were titrated from nanomolars to millimolars (10^{-10}–10^{-3}M) for the dynamic range experiments. These data were further normalized as percentages of FRET relative to the maximal difference of the emission values ($R = R_{max} - R_{min}$). Curve fitting was performed by analyzing the titration experiments. The dissociation constant (K_d) was calculated using the following equation:

$$\Delta R/R = \Delta R1 \times \left[Pb^{2+}\right]/\left(\left[Pb^{2+}\right] + K_{d1}\right) + \Delta R2 \times \left[Pb^{2+}\right]/\left(\left[Pb^{2+}\right] + K_{d2}\right),$$

where ΔR = ratio − R_{min}. For the specificity and competition tests, 1μM of divalent ions (such as $CaCl_2$, $ZnCl_2$, $FeSO_4$, $MgCl_2$, $MnCl_2$, and $CuCl_2$) was used with or without $PbCl_2$ (1μM). The Zn^{2+} effect on Met-lead 1.59 was examined using Pb^{2+} titration (10^{-6}–10^{-4}M) in the presence of Zn^{2+} (1, 0.1, and 0.01μM).

Cell culture and transfection. Human embryonic kidney (HEK293) cells from the American Type Culture Collection (Rockville, MD) were cultured according to the culture manual. The cultured cells were seeded on 24 mm coverglasses (Deckglaser) coated with poly-L-lycine for real-time cellular experiments or on 8-well chamber slides (Lab-Tek) for long-term biomonitoring. The cells were then transfected with pcDNA3_Met-leads using PolyJet (SignaGen Lab, Gaithersburg, MD). The cells were used for cellular experiments after 2 days of transfection.

Emission ratiometric imaging. Emission ratio signals were acquired through an existing ratio-imaging platform including reagent treatments (Chang *et al*., 2008; Chiu *et al*., 2009) with some modifications. The microscope (IX-71, Olympus, Japan) was equipped with a 40× oil objective (NA = 1.35, U/340). A monochrometer (Polychrome V, TILL Photonics, Germany) served as the excitation source (435 nm) and contained a filter cube (excitation band pass = 400–440 nm; dichroic mirror = 455 nm). To acquire the ratio images of the Met-leads within living cells, both fluorescent images of CFP (ECFP(ΔC11)) and YFP (cp173Venus) were captured under a dual charge–coupled device camera system (ORCA-D2, Hamamatsu, Japan). The camera system was equipped with dual-wavelength filters inside the built-in optic blocker for CFP (483/32 nm) and YFP (542/27 nm). The HCImage (Hamamatsu, Japan) software was used to record the FRET ratio images. The emission images of both CFP and YFP within the Met-lead–transfected cells were acquired and assayed in an FRET ratio manner. The FI value of the YFP channel was divided by that of the CFP channel (YFP/CFP) after background subtraction. Ratio imaging was further displayed in a ratio color plate using the analysis software ImageJ (National Institutes of Health). A loading buffer (150mM NaCl, 5mM KCl, 1mM $MgCl_2$, 2.2mM $CaCl_2$, 10mM 4-(2-hydroxyethyl)-1-piperazineethanesulfonic acid, and 5mM D-glucose; pH 7.4) was used for the long-term Pb^{2+} biomonitoring. A loading buffer without Ca^{2+} was used for the ionomycin and thapsigargin (TG) applications.

Data analyses and statistics. All experiments were carried out thrice with at least three different sets of cell samples. Data gathered from the different batches were integrated to calculate the emission ratio. Significant changes were indicated based on a p value calculated using the ANOVA through the LSD (Least Significant Difference, equivalent to no adjustments) and *post hoc* tests (Scheffe) adjustments for multiple comparisons (IBM SPSS statistics 19). The mean difference is significant at the 0.05 level (unless otherwise indicated).

RESULTS

Development of the FRET-Based Pb^{2+} Biosensors

In *C. metallidurans* CH34, PbrR is a gene regulator within the lead ion resistance (*pbr*) operon complex found in the mega-plasmid pMOL30 (Borremans *et al*., 2001). The other two isoforms, $PbrR_2$ and $PbrR_3$, exist in chromosome 1 of CH34 (Taghavi *et al*., 2009). The sequence alignment and comparison of all PbrRs are shown in Figure 1A. All PbrRs contain six α-helix structures (α1–α6, shaded). The three cysteine residues (marked with triangles) were the proposed Pb^{2+}-binding regions (Brown *et al*., 2003). Part of the PbrRs (from the fourth (α4) to sixth (α6) α-helices) designed as the PbBD was incorporated between the FRET protein pair ECFP(ΔC11) and cp173Venus (Nagai *et al*., 2004). The purpose was to build a series of FRET-based Pb^{2+} indicator constructs called Met-leads (Fig. 1B).

PbrRs belong to the MerR family, which can specifically bind metal ions and activate transcription by distorting the DNA (Frantz and O'Halloran, 1990). Such MerR-like proteins are known to form homodimers and thereby generate one pair of ion-binding sites at the two distant edges of the structure unit (Guo *et al*., 2010; Song *et al*., 2007). Based on the above information, the schematic structure and sensing mechanism of Met-leads were proposed and shown in Figure 1C. The key to successful Pb^{2+} sensing by Met-leads relied on the significant conformational changes of PbBD-Pb^{2+} to drive the FRET event in the presence of Pb^{2+} (Fig. 1C).

Spectral Characteristics of the New Met-Leads

The three newly developed Met-leads 1.59, 2.58, and 3.62 were named in numbers to represent their PbBDs originally from PbrR, $PbrR_2$, and $PbrR_3$, respectively. The pattern changes in the emission spectra of the Met-leads at two FI peaks (535 nm for cp173Venus and 475 nm for ECFP(ΔC11)) between the control (without Pb^{2+}; denoted by solid lines in Figs. 2A–C) and Pb^{2+} sample solution (dotted line in Fig. 2A for 1μM; dashed lines in Figs. 2A–C for 100μM) indicated the

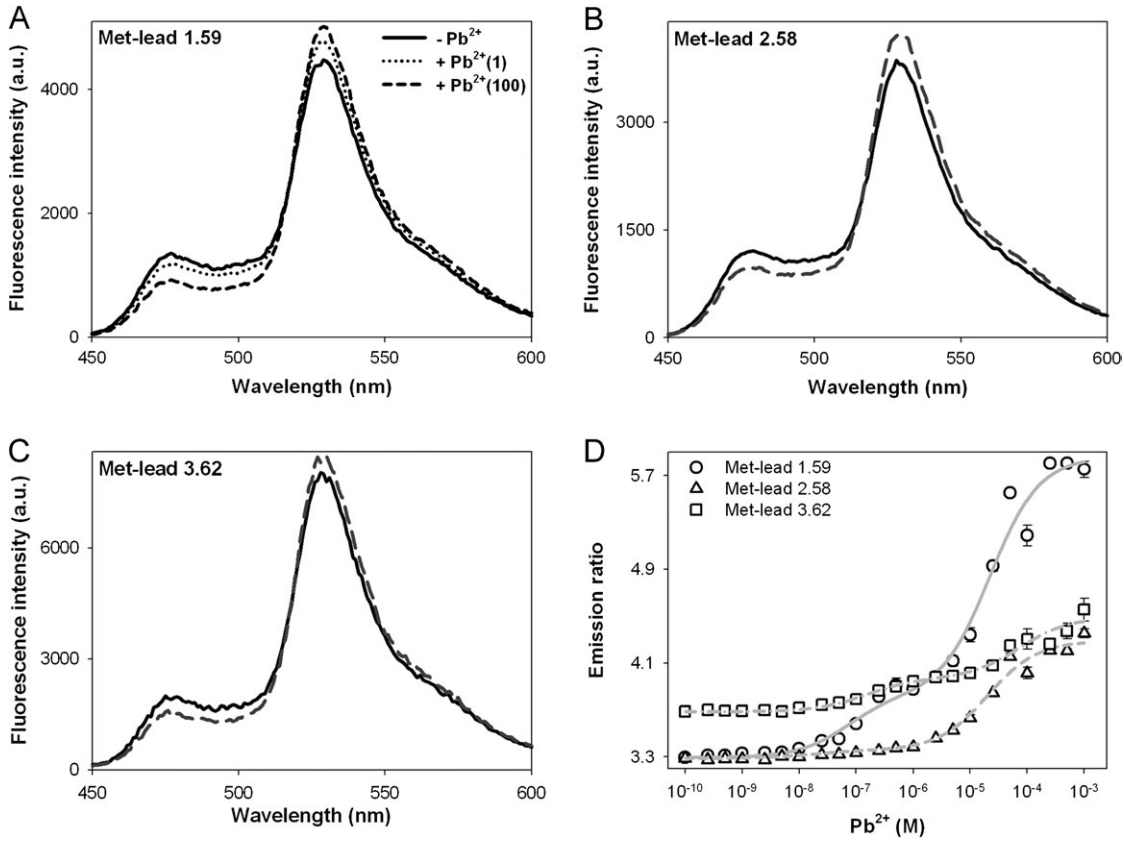

FIG. 2. *In vitro* properties of Met-leads. (A–C) The fluorescence spectral pattern of Met-leads 1.59 (A), 2.58 (B), and 3.62 (C) under various concentrations of lead. All Met-leads contain two fluorescent intensity peaks (475 and 535 nm), indicating the existence of CFP and YFP. The pattern of changes among the solid (without Pb^{2+}), dotted (1μM Pb^{2+} in Met-lead 1.59; A), and dashed (100μM Pb^{2+}) lines further represents the FRET events. (D) The dynamic range of the Met-leads expressed as emission ratios (YFP/CFP): Met-lead 1.59 (closed circle), Met-lead 2.58 (triangle), and Met-lead 3.62 (rectangle). The ranges were recorded after the titration of Pb^{2+} (10^{-10}–10^{-3}M).

occurrence of the successful Pb^{2+}-dependent FRET event. The spectral results in Figures 2A–2C implied that all the Met-leads were capable of sensing Pb^{2+}.

To determine the dynamic range of each Met-lead on Pb^{2+} sensing, the spectral data of Met-leads were further analyzed as the FRET emission ratio (YFP/CFP) under different Pb^{2+} concentrations (10^{-10}–10^{-3}M). The titration curves (Pb^{2+} concentration vs. emission ratio) of Met-leads 1.59, 2.58, and 3.62 are shown in Figure 2D. The dynamic ranges of Met-leads 1.59, 2.58, and 3.62 in terms of emission ratios were 3.3–5.7 (circle), 3.3–4.3 (triangle), and 3.7–4.5 (rectangle), respectively. The titration data (circle, triangle, and rectangle) and the corresponded fitting curve (solid, dashed, and dashed-dotted lines) of each Met-lead construct were further merged together with the emission axes (left side scale, ratio values) and the percentage of FRET axes (right side scale, %), respectively (Supplementary figure S1). The dissociation constants (K_d) of all Met-leads were therefore estimated through the curve fitting as described in the Materials and Methods section. The values of K_{d1} and K_{d2} were 69nM and 22.081μM for Met-lead 1.59 (solid line in Supplementary figure S1A), 18nM and 20.241μM for Met-lead 2.58 (dashed line in Supplementary figure S1B), as well as 149nM and 73.699μM for Met-lead 3.62 (dashed-dotted line in Supplementary figure S1C).

Ion Selectivity of Met-Leads

Molecular specificity is an important requirement for metal ion sensing. The ion selectivities of the developed Met-leads were then challenged to determine the best for Pb^{2+} sensing. The emission ratio changes of the Met-leads (1μM) under the control (H_2O) or selected divalent ions (1μM), e.g., Ca^{2+}, Mg^{2+}, Mn^{2+}, Fe^{2+}, Cu^{2+}, and Zn^{2+}, were compared with those under Pb^{2+} alone (black bars in Fig. 3; the ion selectivity test) or Pb^{2+} combined with the selected ions (empty bars in Fig. 3; the competition test). The increase was about 0.5 for Met-lead 1.59, < 0.1 for Met-lead 2.58, and about 0.2 for Met-lead 3.62. The results indicated that Pb^{2+} can induce a significant increase in the FRET emission ratio even under the background of most tested ions.

The cysteine residues within the MDB of MerR can also recognize Zn^{2+} (Song *et al.*, 2004). The elevated emission ratios of all Met-leads by Zn^{2+} (Figs. 3A–C) agreed with the

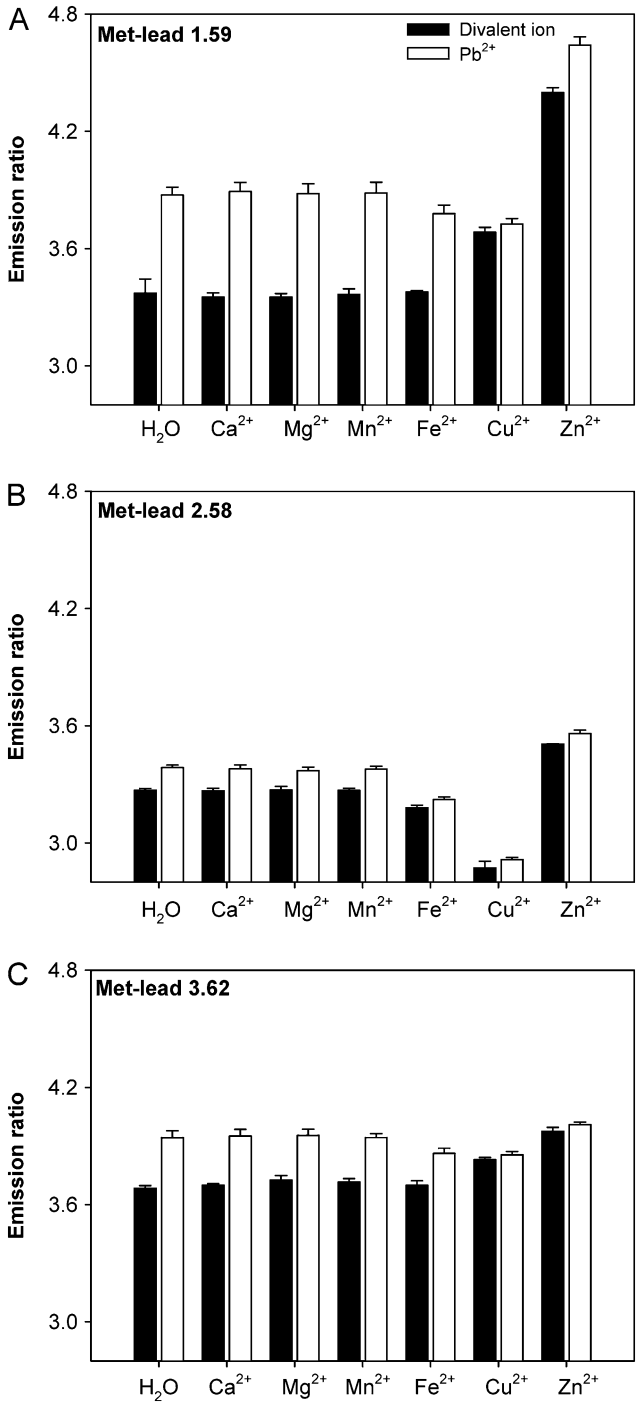

FIG. 3. Ion selection of Met-leads. The sensing abilities of Met-leads 1.59 (A), 2.58 (B), and 3.62 (C) (1μM) were tested on various ions to determine their relative specificities to Pb^{2+}. The tested divalent ions (1μM) were Ca^{2+}, Mg^{2+}, Mn^{2+}, Fe^{2+}, Cu^{2+}, and Zn^{2+} with (empty bars) or without (black bars) Pb^{2+}. Through the LSD ANOVA adjustments for multiple comparisons on each Met-lead construct, the emission ratio with the existence of Pb^{2+} (empty bars) was found to be higher than that without Pb^{2+} (black bars) significantly ($p < 0.0001$). Except for Zn^{2+} and Cu^{2+}, all the above significance is found to be simply related to Pb^{2+} (for details on the effects of Zn^{2+} and Cu^{2+}, please refer to Fig. 4 and Supplementary figure S2).

previous result that Zn^{2+} may also be sensed by other MerR family proteins. Via spectral analyses, this Zn^{2+}-increased basal ratio was found to be indeed due to the real FRET event (dashed line compared with the solid line Apo-control on Met-lead 1.59 in Fig. 4A). Despite the effect of Zn^{2+}, both Met-leads 1.59 and 2.58 can still significantly sense Pb^{2+} with Zn^{2+} (empty bar in the Zn^{2+} parts of Figs. 3A and B). Zn^{2+} may affect the Pb^{2+} sensing ability of Met-leads. Consequently, we tested the Pb^{2+} response (titrated from 10^{-6} to 10^{-4}M) of Met-lead 1.59 under various levels of Zn^{2+} (from as low as 0.01μM in inverse triangle, 0.1μM in open circle, to a relatively high level of 1μM in close circle; Fig. 4B). The emission ratio of Met-lead 1.59 under the presence of nanomolar Zn^{2+} (similar with Fig. 2D) increased from 4 to 6 with the sequential increase of titrated Pb^{2+}. The result implied that the physiological content of Zn^{2+} (from picomolar to nanomolar ranges, Williams and Fraústo da Silva, 2000) did not affect the FRET ratio response of Met-lead 1.59 to Pb^{2+} during the cellular applications.

On the other hand, the spectral data indicated that both Cu^{+} (1μM) and Cu^{2+} (1 and 10μM) cause a fluorescent quenching effect on Met-lead 1.59 (Supplementary figure S2A). Such $Cu^{+/2+}$-induced effect possibly abolished the expected FRET ratio changes and may therefore explain why Pb^{2+} only slightly increased the FRET ratio under the presence of 1μM Cu^{2+} (Fig. 3). The two essential trace elements Zn^{2+} and Cu^{2+} are normally maintained at extremely low levels in living cells (Williams and Fraústo da Silva, 2000). Hence, the only concern of Met-lead 1.59 ion selectivity is Cu^{2+} under a relatively high background level (1μM). In summary, Met-lead 1.59, with its relatively superior dynamic range (Fig. 2D) and fair ion selectivity (compare Figs. 3A–C; Supplementary figure S2D, S3 indicating no influence of Ca^{2+}, Mg^{2+} Mn^{2+}, and Fe^{2+} on Met-lead 1.59), was suitable as a cellular Pb^{2+} indicator for the subsequent live-cell ion imaging.

Visualization of Pb^{2+} Inside Living Cells

HEK293 cells expressing Met-lead 1.59 were placed onto the live-cell imaging system, which gathered the cellular images from both the YFP (Fig. 5A, upper) and CFP (Fig. 5A, middle) channels. The emission ratio images were obtained by dividing the FI of YFP with that of CFP in each pixel (detailed in Materials and Methods section). The images were then displayed in ratio color (Fig. 5A, bottom; the color bar is from 3 to 7 in ratio; color available online). To artificially increase cytosolic Pb^{2+}, 100μM Pb^{2+} containing 5μM ionomycin (Erdahl *et al.*, 2000) was applied. The membrane-permeable Pb^{2+}chelator *N,N,N′,N′*-tetrakis-(2-pyridylmethyl)ethylenediamine (TPEN) (Kerper and Hinkle, 1997) was used to decrease the cytosolic Pb^{2+} (until the end of recording). Sequential changes in the ratio color were significantly observed (from 0 to 60 s at the bottom of Fig. 5A, and also in Supplementary movie 1). The image color changed from blue to red when the

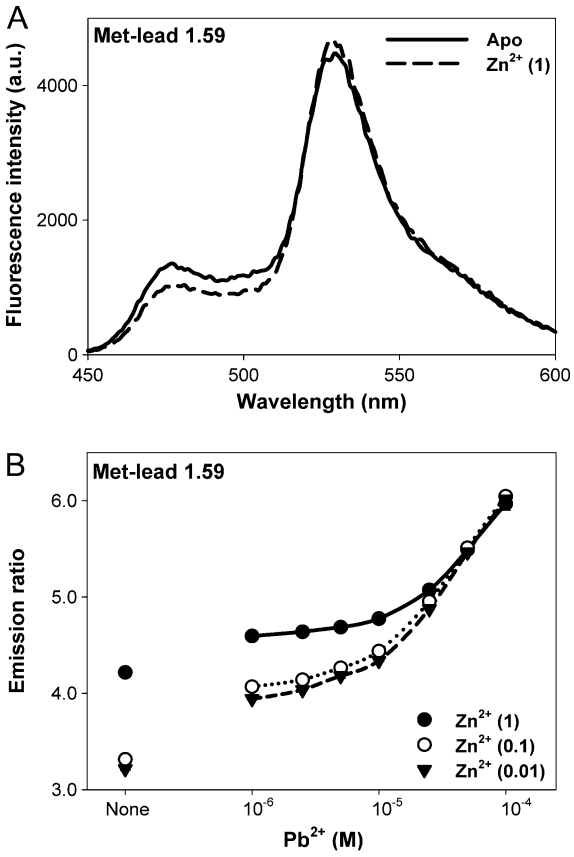

FIG. 4. Effects of Zn^{2+} on the Pb^{2+} sensing of Met-lead 1.59. (A) The spectral patterns of Met-lead 1.59 to Zn^{2+} (1μM; dashed line) compared with the control without specific ions (Apo; solid line). (B) The emission ratios of Met-lead 1.59 under various concentrations of Zn^{2+} (1μM denoted by the close circle, 0.1μM by the open circle, and 0.01μM by the close-inverted triangle) are shown in the left part (none). The titration curves of Met-lead to Pb^{2+} (10^{-6}–10^{-4} M) in the presence of Zn^{2+} (with the three concentrations above) are shown on the right part. The solution of Apo set is the same as others except without the ions Zn^{2+} and Cu^{2+}. Through the multiple comparisons (*post hoc* tests by Scheffe), the emission ratios of Met-lead 1.59 were found to be significantly increased by Pb^{2+} even when different concentrations of Zn^{2+} exist ($p < 0.0001$).

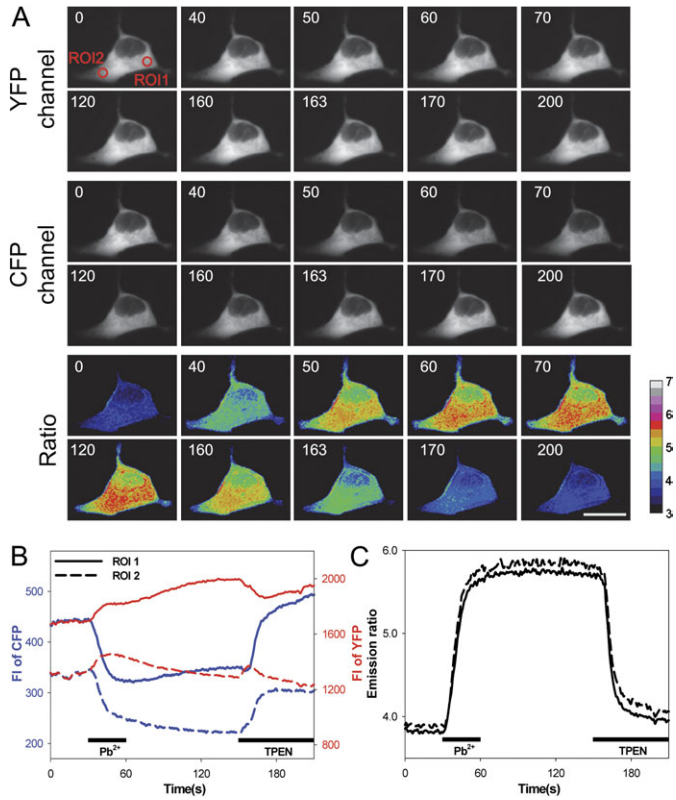

FIG. 5. Live-cell monitoring of intracellular Pb^{2+} content using Met-lead 1.59. (A) The time-lapse fluorescent images of a single HEK293 cell-expressed Met-lead 1.59. Within 200 s of recording, a 100μM Pb^{2+}buffer (containing 5μM ionomycin) was added at the 30-s time point for 30 s. The Pb^{2+}chelator TPEN (100μM) was added at the 150-s time point until the end of the recording (second bar in B and C). The representative images of YFP (10 graphs, upper), CFP (middle), and their ratio (YFP/CFP, bottom) are shown. Two ROIs are selected (ROI 1 is denoted by the solid lines in B and C; ROI 2 is denoted by the dashed lines in B and C). The scale bar is 10 μm. The ratio is from 3 to 7. In (B) and (C), the plots from the two ROIs are displayed as FIs (B) and emission ratios (C).

cells were exposed to Pb^{2+} (after ~30 s) and then changed back from red to blue when TPEN was added (after ~140 s).

Two regions of interest (ROIs) were selected within the same tested cell (ROI 1 and ROI 2; red circles in Fig. 5A, available in color online) to demonstrate the time-lapse quantity of FI in CFP (blue lines in Fig. 5B, available in color online) and YFP (red lines in Fig. 5B, available in color online). In the presence of Pb^{2+}, the FI of YFP and the emission ratios increased, whereas those of CFP decreased. The emission ratios shown in Figure 5C indicated that the existence of the FRET event was correlated with increased cytosolic Pb^{2+}. TPEN reversed the Pb^{2+} response of Met-lead 1.59. The ratio color images together with the line plots directly demonstrated the dynamics of cytosolic Pb^{2+}. The live-cell dynamic ranges (as emission ratio changes) of Met-leads 1.59, 2.58, and 3.62 expressed in the HEK293 cells were 3.9–5.8, 3.7–5.4, and 3.8–4.5, respectively (Supplementary figure S6).

Cytosolic Pb^{2+} Entry Enhancement by Activated SOCE

Met-lead 1.59 was also used to sense the cytotoxic entry of Pb^{2+} at resting or activated SOCE states (Fig. 6) after the above Met-lead performance determination using ionomycin inside living cells. Slightly increased emission ratios caused by the two different Pb^{2+} concentrations (10 and 50μM) were shown through both the ratio image display (Fig. 6A) and ratio plots (Fig. 6B) of the Met-lead 1.59–expressed cells. The comparison of the dynamic contents of intracellular Pb^{2+} under exposure to various concentrations of Pb^{2+} (10μM denoted by the dotted gray line and 50μM by the dashed gray line in Fig. 6B) with the control status (solid gray line) were recorded within 5 min. TG was used to activate SOCE by emptying the

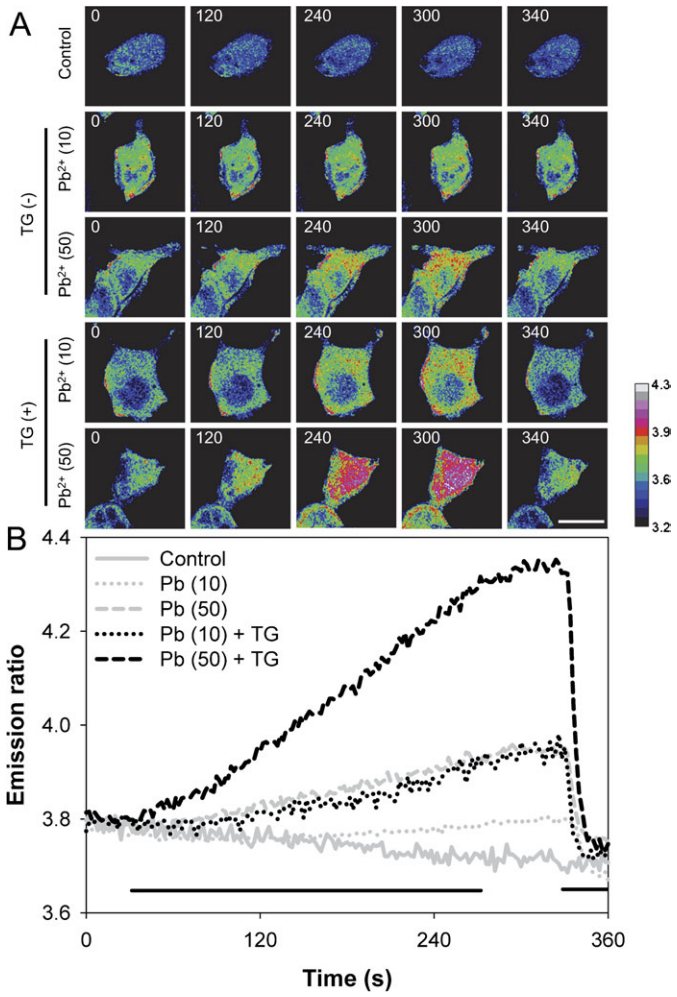

FIG. 6. Cytosolic entry of Pb^{2+} correlated to the functional activity of SOCE. (A) and (B) The time-lapse ratio data of each representative Met-lead 1.59-expressed cell are shown in both the sequential images (A) and line plots (B). During the 360 s of short-term recording, 10μM (dotted lines) or 50μM (dashed lines) of Pb^{2+} was added (first bar) for 240 s from the 30-s time point with (black lines) or without (gray lines) TG 20 min prior to the experiments (Supplementary figure S4). At the end of the recording, TPEN was used (the second bar) to ensure that the increased ratio was due to the existence of Pb^{2+}. The control set (solid gray line) was for the loading buffer with the same duration. The emission ratio difference between the time point (29 and 329 s) of Pb^{2+} treatment under various conditions (with or without TG) was analyzed under pairwise comparisons ($p < 0.05$).

endoplasmic reticulum (ER) Ca^{2+} store. Under this TG-activated SOCE condition, the cytotoxic Pb^{2+} entry was found to be significantly enhanced compare with TG-untreated set (10μM, shown by the dotted black line, and 50μM, shown by the dashed black line). This Pb^{2+} response was also reversible using TPEN. These data further demonstrated the enhanced role of SOCE on cytotoxic Pb^{2+} entry under transient exposure. Therefore, Met-lead 1.59 was proven capable in selectively detecting intracellular Pb^{2+} content in living cells. The cellular imaging test on the ability of the Met-leads in sensing Pb^{2+} was successful.

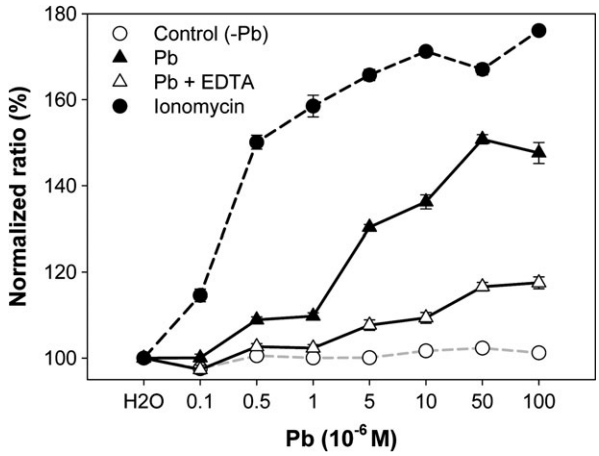

FIG. 7. Cytosolic content of Pb^{2+}still remaining inside living cells during long-term exposure. Met-lead 1.59-expressed cells were tested after 3 h of Pb^{2+} exposure. The normalized emission ratios (%) are shown under different concentrations of Pb^{2+} (0.1–100μM) alone (closed triangles), with additional EDTA treatment (500μM) after Pb^{2+} exposure (open triangles), or with ionomycin (closed circles). The gray dash line (with open circles) represents the control cells before the addition of Pb^{2+} (and of the others) as the background ratio level. Through *post hoc* tests (Multiple Comparisons, Scheffe), the normalized emission ratios of Met-lead 1.59 with Pb^{2+} (from 0.5μM) were found to be significantly higher than that without Pb^{2+} (H_2O) ($p < 0.0001$). The additional treatment of EDTA further significantly decreased such elevated response ($p < 0.0001$, LSD Multiple Comparisons).

Long-Term Monitoring of Intracellular Pb^{2+} Content

Measuring the intracellular content of Pb^{2+} with Met-lead 1.59 through certain long time (e.g., 3 h or even longer) of exposure with various levels (even under the BLL borderline) is a good way to investigate the dynamics of Pb^{2+} within living cells in the view of ion traffic and accumulation, i.e., the sum of exposure (the balance of uptake/entry and excretion) after continuously exposure. The capability of the Met-leads to sense Pb^{2+} chronically under similar clinical conditions, i.e., 0.5μM exposure of Pb^{2+} (a little higher than the BLL borderline, 10 μg/dl) (CDC, 1991) were next determined. Met-lead 1.59–expressed cells were bathed with various Pb^{2+} concentrations (0.1–100μM) for at least 3 h, and the Pb^{2+} content inside these cells were measured (Fig. 7). The results indicated that Met-lead 1.59 sensed Pb^{2+} content after low levels (0.5μM) of 3-h long-term Pb^{2+} exposure (compare the close triangles with the open circles in Fig. 7). Ionomycin (5μM) combined with a defined Pb^{2+} solution was used for the intracellular Pb^{2+} titration (close circles). Given that EDTA is one of the clinical treatments for Pb^{2+} poisoning (CDC, 1991), EDTA was applied on the Pb^{2+}-exposed cells. As shown in Figure 7 (compare the open triangles with the closed triangles), 500μM EDTA significantly decreased the intracellular levels of Pb^{2+} under all exposed concentrations.

DISCUSSION

Information on BLLs is thus far the only clinical diagnosis tool available for showing different levels of Pb^{2+} poisoning.

This tool provides a warning and allows the prevention of excessive Pb^{2+} exposure in human bodies and suggests proper medical treatments. As aforementioned, the acceptable BLL is below 10 μg/dl (CDC, 1991), whereas there is no absolute clinical symptom under the so-called poisonous BLL. The measured BLL actually represents the estimated amount of Pb^{2+} existing not only in physiological fluids circulating in the entire whole human body (i.e., the extracellular part) but also in the cytosolic space of each cell. In fact, the intracellular portion that is directly correlated to the major cytotoxic effects of Pb^{2+} has always been diluted and masked by the extracellular Pb^{2+} content in BLLs. Intracellular Pb^{2+} monitoring has been overlooked for years; hence, BLL values are still continuously downward revised (CDC Advisory Committee on Childhood Lead Poisoning Prevention, 2007). Any kind of tool that can aid in accurately determining the harmful level of intracellular Pb^{2+} is urgently needed.

Chemical- and protein-based heavy metal ion indicators for both environmental (extracellular) Pb^{2+} detection (Chen and Huang, 2002; Chen *et al*., 2005; Marbella *et al*., 2009) and live-cell studies (He *et al*., 2006; Kerper and Hinkle, 1997; Mizuno *et al*., 2007; Richmond *et al*., 2000) have been extensively fabricated. For extracellular Pb^{2+} sensing, some small-molecule fluorescent indicators are very highly sensitive to Pb^{2+} (Chen and Huang, 2002; Marbella *et al*., 2009). However, due to their molecular characteristics, such as incompatibility with water and instability within the cytosolic space, only a limited number of chemical detectors are capable of sensing cytosolic Pb^{2+} (He *et al*., 2006). In the present study, protein-based Pb^{2+} indicator(s) that function inside living cells were constructed to overcome the limitations of the chemical ones. The newly developed FRET-based Pb^{2+} indicator, Met-lead 1.59, was a workable tool that can provide content measurement of intracellular Pb^{2+} under experimental long-term (at least 3 h) exposures with various extracellular Pb^{2+} concentrations (Fig. 7). Future detections of intracellular Pb^{2+} content hiding within the BLL using this Pb^{2+} indicator or an alternative warrant further investigations.

Intracellular Pb^{2+} content was successfully and practically detected by Met-lead 1.59 during at least a 3-h exposure with as low as 0.5μM, which is equal to ~10 μg/dl (Fig. 7). This range was about 200 times lower than those used in previous studies, i.e., 100μM (Chang *et al*., 2008; Chiu *et al*., 2009; White *et al*., 2007). Clearly, the sensitivity of Met-lead 1.59 was sufficiently high for advanced studies, such as the chronic content monitoring of intracellular Pb^{2+} in human cells under continuously contaminated environments, e.g., a lead-containing diet or work area.

Apparently, the intracellular amount of Pb^{2+} within HEK293 cells is equal to the extracellular concentration of 0.5μM (almost reached to 50μM, i.e., 1 mg/dl, 100 times the acceptable BLL) after 3 h of 50μM exposure (compare the close triangle at the 50μM point and close circle at the 0.5μM point in Fig. 7). The intracellular Pb^{2+} concentration of 0.5–50μM may be the buffering range that healthy cells can temporarily bear throughout the long-term exposure. An alternative explanation for this phenomenon is that there may exist an unidentified protection mechanism like organelle sequestration, e.g., mitochondria (Walton, 1973) or ER (White *et al*., 2007), that buffers the increased amount of intracellular Pb^{2+}. Given that our newly developed Met-leads were protein-based, they have a great potential to be organelle targeted and can be applied in subcellular tracing studies to address this issue in the near future.

MerR has been originally found within the Hg^{2+} resistance *mer* operon of Gram-negative bacteria (Barrineau *et al*., 1985). As a transcriptional activator, MerR can specifically bind Hg^{2+}, distort DNA, and activate the transcriptional process (Frantz and O'Halloran, 1990). Other MerR family members such as ZntR (Outten and O'Halloran, 2001), CueR (Changela *et al*., 2003), and PbrR (Borremans *et al*., 2001) from different bacterial strains were also found to have similar gene regulatory functions after a highly specific binding with Zn^{2+}, Cu^{+}, and Pb^{2+}, respectively. Chen *et al*. (2005) have recently used the intact $PbrR_2$ protein combined with a specific DNA fragment (as transcription promoters) to develop a novel extracellular Pb^{2+}-specific DNAzyme probe (Chen *et al*., 2005). The 80 to 128 residues of MerR were found to be the smallest region (only 30% of MerR) that forms a stable dimer while preserving the highly selective binding affinity to Hg^{2+} (Zeng *et al*., 1998). Consequently, PbrR is proposed to be a good material for constructing an FRET-based Pb^{2+} indicator for intracellular sensing. In the present study, the PbBD of PbrR (without the DNA biding part) was applied as a sensing key to develop the FRET-based Pb^{2+} indicator. Experimentally, all three PbBDs were found capable of making sufficient conformational changes to drive the FRET event upon Pb^{2+} binding (Figs. 2A–C). The success of the Met-leads in live-cell Pb^{2+} sensing (completely seen in Supplementary Figure 1) is assumed to be due to the ability of PbBD in both specific Pb^{2+} binding and the driving of the significant FRET event between CFP and cpVenus. Perhaps, the MerR family proteins can be used in future studies to fabricate a series of metal ion indicators, such as those for Hg^{2+}, Cd^{2+}, and even Zn^{2+} (Supplementary figure S5).

Finally, regarding the gateway issue of Pb^{2+}, two candidates other than Orai1/CRACM1 and STIM1 will be tested by Met-lead 1.59 in the near future. One is the divalent metal transporter 1, which was previously proposed to be the gateway of Pb^{2+} uptake in an acidic environment, such as the gastrointestinal tract (Bannon *et al*., 2002). The other is the transient receptor potential, another SOC component, which may also be a possible gateway for Pb^{2+} entry. The possible detoxification mechanism in humans (if naturally existing) is also thus far mysterious. With the newly developed intracellular Pb^{2+} sensor Met-lead 1.59, more experiments should be carried out to examine the above issues.

In summary, a newly constructed FRET-based Pb^{2+} indicator, Met-lead 1.59, is ready for advanced research on Pb^{2+}.

This valuable tool can aid further investigations on the molecular, cellular, and even subcellular toxicology of Pb^{2+}. To date, the intracellular part of Pb^{2+} is still hidden within the total content of BLL. The results of the present study suggest that intracellular Pb^{2+} should be extracted out of BLL as a new valuable item for further clinical evaluations.

SUPPLEMENTARY DATA

Supplementary data are available online at http://toxsci.oxfordjournals.org/.

FUNDING

National Science Council of the Republic of China, Taiwan (NSC-97-2320-B-075-005-MY3, NSC-100-2320-B-075-004); Taipei Veterans General Hospital (V98C1-052, V99C1-002, V100C1-032); Joint Projects of UTVGH; National Yang-Ming University (Ministry of Education, Aim for the Top University Plan).

ACKNOWLEDGMENTS

The authors would like to thank Professor Takeharu Nagai for the generous sharing of YC 3.6. We also appreciate Prof. Daniel van der Lelie kindly providing the bacteria *C. metallidurants* CH34. T.Y.C. thanks Professors Lung-Sen Kao, Yijuang Chern, Chao-Tsen Chen, Chih-Chang Juan, and Takeharu Nagai for valuable suggestions for this study. The authors thank Ms Li-Chun Wang and Chi-Shu Liao for the technical support.

REFERENCES

Bannon, D. I., Portnoy, M. E., Olivi, L., Lees, P. S., Culotta, V. C., and Bressler, J. P. (2002). Uptake of lead and iron by divalent metal transporter 1 in yeast and mammalian cells. *Biochem. Biophys. Res. Commun.* **295,** 978–984.

Barrineau, P., Gilbert, P., Jackson, W. J., Jones, C. S., Summers, A. O., and Wisdom, S. (1985). The structure of the mer operon. *Basic Life Sci.* **30,** 707–718.

Borremans, B., Hobman, J. L., Provoost, A., Brown, N. L., and Van der Lelie, D. (2001). Cloning and functional analysis of the pbr lead resistance determinant of *Ralstonia metallidurans* CH34. *J. Bacteriol.* **183,** 5651–5658.

Brown, N. L., Stoyanov, J. V., Kidd, S. P., and Hobman, J. L. (2003). The MerR family of transcriptional regulators. *FEMS Microbiol. Rev.* **27,** 145–163.

CDC Advisory Committee on Childhood Lead Poisoning Prevention (2007). Interpreting and managing blood lead levels < 10 microg/dL in children and reducing childhood exposures to lead: Recommendations of CDC's Advisory Committee on Childhood Lead Poisoning Prevention. *MMWR Recomm Rep.* **56,** 1–16.

Centers for Disease Control and Prevention (CDC) (1991). *Preventing Lead Poisoning in Young Children*. U.S. Department of Health and Human Services, Atlanta, GA.

Chang, Y. F., Teng, H. C., Cheng, S. Y., Wang, C. T., Chiou, S. H., Kao, L. S., Kao, F. J., Chiou, A., and Yang, D. M. (2008). Orai1-STIM1 formed store-operated Ca^{2+} channels (SOCs) as the molecular components needed for Pb^{2+} entry in living cells. *Toxicol. Appl. Pharmacol.* **227,** 430–439.

Changela, A., Chen, K., Xue, Y., Holschen, J., Outten, C. E., O'Halloran, T. V., and Mondragón, A. (2003). Molecular basis of metal-ion selectivity and zeptomolar sensitivity by CueR. *Science* **301,** 1383–1387.

Chen, C. T., and Huang, W. P. (2002). A highly selective fluorescent chemosensor for lead ions. *J. Am. Chem. Soc.* **124,** 6246–6247.

Chen, P., Greenberg, B., Taghavi, S., Romano, C., van der Lelie, D., and He, C. (2005). An exceptionally selective lead(II)-regulatory protein from *Ralstonia metallidurans*: Development of a fluorescent lead(II) probe. *Angew. Chem. Int. Ed. Engl.* **44,** 2715–2719.

Chiu, T. Y., Teng, H. C., Huang, P. C., Kao, F. J., and Yang, D. M. (2009). Dominant role of Orai1 with STIM1 on the cytosolic entry and cytotoxicity of lead ions. *Toxicol. Sci.* **110,** 353–362.

Erdahl, W. L., Chapman, C. J., Taylor, R. W., and Pfeiffer, D. R. (2000). Ionomycin, a carboxylic acid ionophore, transports Pb(2+) with high selectivity. *J. Biol. Chem.* **275,** 7071–7079.

Frantz, B., and O'Halloran, T. V. (1990). DNA distortion accompanies transcriptional activation by the metal-responsive gene-regulatory protein MerR. *Biochemistry* **29,** 4747–4751.

Guo, H. B., Johs, A., Parks, J. M., Olliff, L., Miller, S. M., Summers, A. O., Liang, L., and Smith, J. C. (2010). Structure and conformational dynamics of the metalloregulator MerR upon binding of Hg(II). *J. Mol. Biol.* **398,** 555–568.

He, Q., Miller, E. W., Wong, A. P., and Chang, C. J. (2006). A selective fluorescent sensor for detecting lead in living cells. *J. Am. Chem. Soc.* **128,** 9316–9317.

Kerper, L. E., and Hinkle, P. M. (1997). Cellular uptake of lead is activated by depletion of intracellular calcium stores. *J. Biol. Chem.* **272,** 8346–8352.

Li, I. T., Pham, E., and Truong, K. (2006). Protein biosensors based on the principle of fluorescence resonance energy transfer for monitoring cellular dynamics. *Biotechnol. Lett.* **28,** 1971–1982.

Marbella, L., Serli-Mitasev, B., and Basu., P. (2009). Development of a fluorescent Pb^{2+} sensor. *Angew. Chem. Int. Ed. Engl.* **48,** 3996–3998.

Miyawaki, A., Llopis, J., Heim, R., McCaffery, J. M., Adams, J. A., Ikura, M., and Tsien, R. Y. (1997). Fluorescent indicators for Ca^{2+} based on green fluorescent proteins and calmodulin. *Nature* **388,** 882–887.

Mizuno, T., Murao, K., Tanabe, Y., Oda, M., and Tanaka, T. (2007). Metal-ion-dependent GFP emission *in vivo* by combining a circularly permutated green fluorescent protein with an engineered metal-ion-binding coiled-coil. *J. Am. Chem. Soc.* **129,** 11378–11383.

Nagai, T., Yamada, S., Tominaga, T., Ichikawa, M., and Miyawaki, A. (2004). Expanded dynamic range of fluorescent indicators for Ca(2+) by circularly permuted yellow fluorescent proteins. *Proc. Natl. Acad. Sci. U.S.A.* **101,** 10554–10559.

Outten, C. E., and O'Halloran, T. V. (2001). Femtomolar sensitivity of metal-loregulatory proteins controlling zinc homeostasis. *Science* **292,** 2488–2492.

Richmond, T. A., Takahashi, T. T., Shimkhada, R., and Bernsdorf, J. (2000). Engineered metal binding sites on green fluorescence protein. *Biochem. Biophys. Res. Commun.* **268,** 462–465.

Rost, B., Yachdav, G., and Liu, J. (2004). The PredictProtein server. *Nucleic Acids Res.* **32,** W321–W326.

Song, L., Caguiat, J., Li, Z., Shokes, J., Scott, R. A., Olliff, L., and Summers, A. O. (2004). Engineered single-chain, antiparallel, coiled coil mimics the MerR metal binding site. *J. Bacteriol.* **186,** 1861–1868.

Song, L., Teng, Q., Phillips, R. S., Brewer, J. M., and Summers, A. O. (2007). 19F-NMR reveals metal and operator-induced allostery in MerR. *J. Mol. Biol.* **371,** 79–92.

Taghavi, S., Lesaulnier, C., Monchy, S., Wattiez, R., Mergeay, M., and van der Lelie, D. (2009). Lead(II) resistance in *Cupriavidus metallidurans* CH34: Interplay between plasmid and chromosomally-located functions. *Antonie Van Leeuwenhoek* **96,** 171–182.

Vinkenborg, J. L., Koay, M. S., and Merkx, M. (2010). Fluorescent imaging of transition metal homeostasis using genetically encoded sensors. *Curr. Opin. Chem. Biol.* **14,** 231–237.

Walton, J. R. (1973). Granules containing lead in isolated mitochondria. *Nature* **243,** 100–101.

Wegner, S. V., Arslan, H., Sunbul, M., Yin, J., and He, C. (2010). Dynamic copper(I) imaging in mammalian cells with a genetically encoded fluorescent copper(I) sensor. *J. Am. Chem. Soc.* **132,** 2567–2569.

White, L. D., Cory-Slechta, D. A., Gilbert, M. E., Tiffany-Castiglioni, E., Zawia, N. H., Virgolini, M., Rossi-George, A., Lasley, S. M., Qian, Y. C., and Basha, M. R. (2007). New and evolving concepts in the neurotoxicology of lead. *Toxicol. Appl. Pharmacol.* **225,** 1–27.

Williams, R. J. P., and Fraústo da Silva, J. J. R. (2000). The distribution of elements in cells. *Coord. Chem. Rev.* **200-202,** 247–348.

Zeng, Q., Stålhandske, C., Anderson, M. C., Scott, R. A., and Summers, A. O. (1998). The core metal-recognition domain of MerR. *Biochemistry* **37,** 15885–15895.